Earth and Planetary Science Letters 409 (2015) 147–156

Contents lists available at ScienceDirect

Earth and Planetary Science Letters

www.elsevier.com/locate/epsl

An observational and thermodynamic investigation of carbonate partial melting

David Floess [a,b,*], Lukas P. Baumgartner [a], Pierre Vonlanthen [a]

[a] Institute of Earth Sciences, University of Lausanne, Switzerland
[b] Department of Earth Sciences, University of Geneva, Switzerland

ARTICLE INFO

Article history:
Received 22 March 2014
Received in revised form 4 September 2014
Accepted 13 October 2014
Available online xxxx
Editor: T. Elliott

Keywords:
anatexis
carbonate melt
contact metamorphism
melting microstructure
rheology
phase diagram

ABSTRACT

Melting experiments available in the literature show that carbonates and pelites melt at similar conditions in the crust. While partial melting of pelitic rocks is common and well-documented, reports of partial melting in carbonates are rare and ambiguous, mainly because of intensive recrystallization and the resulting lack of criteria for unequivocal identification of melting. Here we present microstructural, textural, and geochemical evidence for partial melting of calcareous dolomite marbles in the contact aureole of the Tertiary Adamello Batholith. Petrographic observations and X-ray micro-computed tomography (X-ray μCT) show that calcite crystallized either in cm- to dm-scale melt pockets, or as an interstitial phase forming an interconnected network between dolomite grains. Calcite–dolomite thermometry yields a temperature of at least 670 °C, which is well above the minimum melting temperature of ~600 °C reported for the CaO–MgO–CO_2–H_2O system. Rare-earth element (REE) partition coefficients ($K_D^{cc/do}$) range between 9–35 for adjacent calcite–dolomite pairs. These K_D values are 3–10 times higher than equilibrium values between dolomite and calcite reported in the literature. They suggest partitioning of incompatible elements into a melt phase. The $\delta^{18}O$ and $\delta^{13}C$ isotopic values of calcite and dolomite support this interpretation. Crystallographic orientations measured by electron backscattered diffraction (EBSD) show a clustering of *c*-axes for dolomite and interstitial calcite normal to the foliation plane, a typical feature for compressional deformation, whereas calcite crystallized in pockets shows a strong clustering of *c*-axes parallel to the pocket walls, suggesting that it crystallized after deformation had stopped. All this together suggests the formation of partial melts in these carbonates.

A Schreinemaker analysis of the experimental data for a CO_2–H_2O fluid-saturated system indeed predicts formation of calcite-rich melt between 650–880 °C, in agreement with our observations of partial melting. The presence of partial melts in crustal carbonates has important physical and chemical implications, including a drastic drop in rock viscosity and significant change in the dynamics and distribution of fluids within both the contact aureole and the intrusive body.

1. Introduction

Igneous intrusions commonly cause partial melting of the surrounding host rock (e.g. Pattison and Harte, 1988; Johnson et al., 2003; Wohlers and Baumgartner, 2013). Hence, temperatures exceeding 650 °C are often attained in contact aureoles, corresponding to the granite solidus. Melting of pelitic rocks results in drastic changes of the physico-chemical properties of the rocks. A strongly reduced viscosity leads to a high melt and element mobility. This influences the deformation behavior of the partially molten rock and typically cause chemical layering (e.g. leucosomes and melanosomes). The recognition of partially molten rocks is therefore crucial.

Many intrusive bodies are hosted in carbonate rocks, and much less is known about potential melting of these carbonates, despite the fact that experiments on melting of carbonates were first performed at the end of the 1950s in the ternary system CaO–CO_2–H_2O. Considering pressure values typical of the upper crust, partial melting of carbonates was observed at temperatures around 740 °C (1 kbar; Wyllie and Tuttle, 1959). Subsequent experimental studies added MgO as fourth component, and the crucial role played by the ratio H_2O–CO_2 in the topology of melting

* Corresponding author at: Department of Earth Sciences, University of Geneva, Rue des Maraichers 13, CH, 1205, Geneva, Switzerland.
E-mail address: david.floess@unige.ch (D. Floess).

http://dx.doi.org/10.1016/j.epsl.2014.10.031
0012-821X/

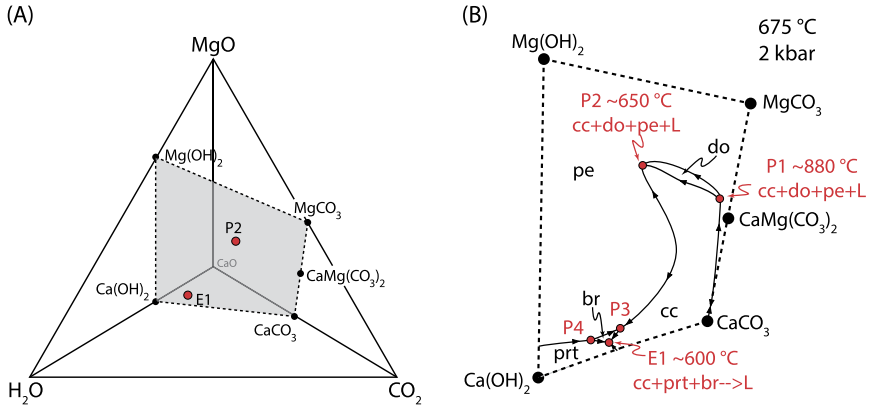

Fig. 1. Phase relationships obtained by Fanelli et al. (1986). (A) Quaternary phase diagram for the components CaO–MgO–CO_2–H_2O. It shows the eutectic E1 and the peritectic P2, at moderate temperatures. (B) Phase diagram for the sub-system, indicated as a grey-shaded area in (A). It is defined by the phases calcite, magnesite, brucite and portlandite. The black solid lines represent the liquidus and the arrows point towards decreasing liquidus temperatures. The experimental conditions were 675 °C and 2 kbar.

reactions was studied (Wyllie and Tuttle, 1960; Wyllie, 1965; Fanelli et al., 1986). Melting of carbonates was reported at temperatures as low as ~600 °C (2 kbar), close to the water-rich end of the CO_2–H_2O join.

Fig. 1A shows the quaternary phase diagram defined by the components CaO, MgO, CO_2 and H_2O, as used by Fanelli et al. (1986). The experiments were carried out in the quadrilateral delimited by the components calcite, magnesite, portlandite and brucite (Fig. 1B). Both the eutectic E1 and the peritectic P2 involve calcite, but only P2 also involves dolomite. The temperature estimates for E1 and P2 are ~600 and 650 °C, respectively. These temperatures are similar, or even below those for partial melting of pelitic rocks. The presence of periclase in metadolomites, and wollastonite and vesuvianite in calcite-dominated lithologies (e.g. Moore and Kerrick, 1976; Cook and Bowman, 2000; Ferry et al., 2002; Nabelek, 2002; Müller et al., 2009) demonstrates that fluids are often very water-rich in carbonates close to the contact, so that abundant partial melting would be expected in dolomitic carbonates. However, very few studies reported indisputable evidence for melting of natural carbonates. Wenzel et al. (2001) invoked carbonate melting for the formation of Mg-rich skarn xenoliths in the Ioko–Dovyren intrusion, Eastern Siberia. Calcium was extracted from the xenoliths by forming a calcite-rich melt leaving behind a periclase-rich restite. The authors use the contamination of the mafic magma by CaO and the virtual absence of Ca in the xenoliths as evidence for partial melting. Another potential occurrence was reported from the New Carlisle area, Canada by Jutras et al. (2006). There, the injection of mafic dikes into wet sediments initiated local melting of carbonates. The occurrence of fragmented dikes in a carbonate matrix and "flow structures" are used to argue for partial melting.

Partial melting of dolomitic carbonates might be much more common than hitherto considered, based on the above studies. The scarcity of studies reporting partial melting in natural carbonates might be due to the lack of criteria to unambiguously identify partial melting in marbles, since the "restite" (dolomite) and the "leucosome" (calcite) can rarely be identified in the field. Further, textures are often obliterated by sub-solidus recrystallization and interaction with fluids. In this study, a wide spectrum of microstructural, geochemical and textural methods were coupled with field observations to provide unambiguous criteria for the recognition of partial melting in crustal carbonates.

2. Geological background and samples

The Western Adamello Tonalite (Northern Italy, Fig. 2A) was emplaced into the South-Alpine basement rocks and the Permo–Triassic cover at ~37.7 Ma (Floess, 2013), causing a distinct contact metamorphic overprint. The host rock PT-conditions prior to intrusion are estimated at 2.5 kbar and a maximum temperature of 250 °C (see discussion by Pennacchioni et al., 2006). The intrusion of the Western Adamello Tonalite caused partial melting of the metapelitic basement rocks up to a distance of 350 m from the intrusive contact (Fig. 2A). The siliciclastic Permian sequence changed gradually with time towards carbonate-dominated sediments. The subhorizontal Permo–Triassic cover sequence was folded downwards and thinned along the contact to form a subvertical sliver, about 200 m in thickness. Comparison with reference stratigraphic sections (Brack, 1984 and references therein) indicates that the sequence underwent at least a 5-fold thinning, largely due to the emplacement of the tonalitic intrusion (Floess, 2013). The sedimentary bedding is overprinted by a metamorphic foliation sub-parallel to the vertical intrusive contact.

Twenty-five samples were collected from the lower and middle Triassic calcite-bearing dolomites and petrographic thin sections were prepared for observation under the polarizing microscope. A slab of each sample was stained using Alizarin Red to facilitate the distinction between calcite (red) and dolomite (white), following the recommendations of Hutchison (1974). Four samples showed conspicuous indications for partial melting. Of these, one sample (DF316) was selected for detailed microstructural, geochemical and textural analysis. The sample was chosen based on microstructures indicating potential partial melting. The sample location is about 50 m from the intrusive contact. The sample consists of dolomite (60 vol.%), calcite (30 vol.%), forsterite (5 vol.%), mica (5 vol.%) and minor amounts of pyrite and apatite. Only one grain of potential brucite (after periclase) was found in thin section. This is noteworthy since brucite replacing periclase is frequently observed elsewhere in high-grade carbonate rocks (e.g. Pattison and Harte, 1997; Ferry et al., 2002; Müller et al., 2009). Calcite can be differentiated from dolomite in hand specimen based on a slightly brighter color and more weathered appearance (Fig. 2D). Calcite occurs either as (1) cm-sized grains crystallized in isolated pockets, up to 20 cm in size (Fig. 2B), (2) pervasive network of interstitial grains within dolomite-rich regions (Fig. 3A–C), or (3) vein-like structures penetrating the calcite–dolomite assemblage (Fig. 2C to D). Dolomite grains are typically a few hundreds of µm in size. They occur mostly in the matrix of the marbles, along with varying amounts of interstitial calcite.

3. Methods

The sample was investigated using FE-SEM, X-ray tomography, EMPA, LA-ICP-MS, stable isotopes and EBSD. A short description

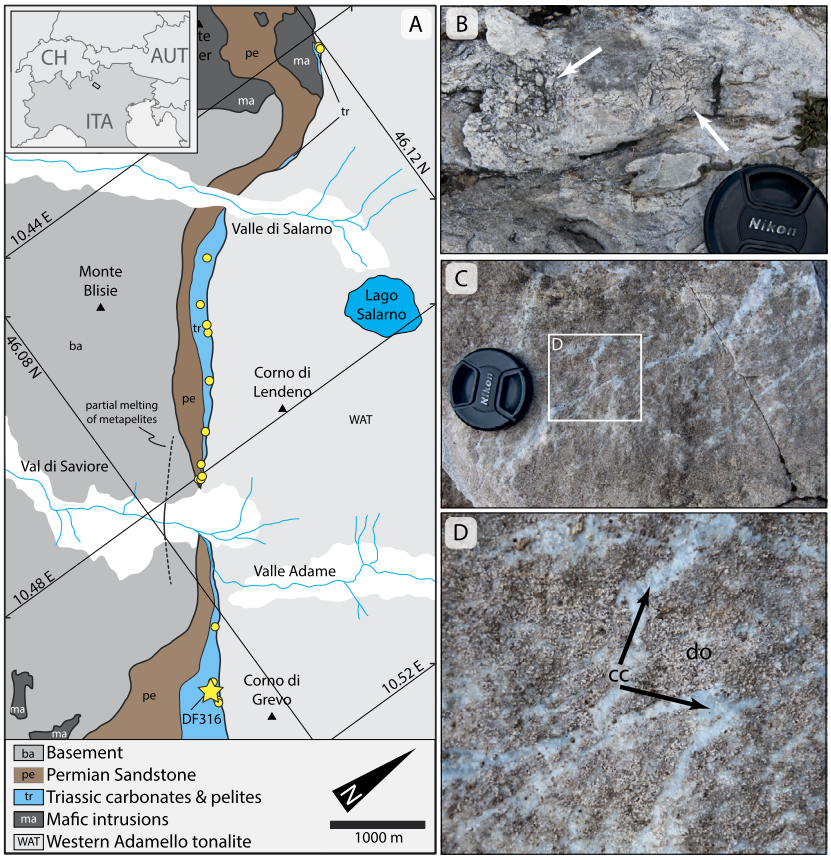

Fig. 2. (A) Simplified geological map of the Western Adamello contact aureole (modified from Brack et al., 2008). Small circles indicate sample locations; the sample DF316 (star) was studied in detail. Partial melting of carbonates occurs only within about 50 m of the intrusive contact with the tonalite intrusion. (B to D) Field photographs showing possible indicators of partial melting. (B) Cm-sized crystals of calcite in isolated melt pockets (arrows). (C) Irregular vein-like structure criss-cross the dolomite marble. (D) Close-up view of (C) showing bright calcite vein (arrows) cutting a slightly darker dolomite-rich region.

of the salient measurement conditions is given below. All analyses were performed at the University of Lausanne, Switzerland.

Backscattered electron (BSE) images were taken using a Tescan Mira LMU field emission-scanning electron microscope (FE-SEM) operated at an acceleration voltage of 15 kV and a probe current of 1.4 nA. Seven BSE images (0.36 to 2.53 mm^2) were processed using the ImageJ software (Schneider et al., 2012). Successive steps of grayscale thresholding were used to identify and separate carbonate phases prior to area calculations.

The 3D distribution of calcite and dolomite based on their respective difference in X-ray attenuation coefficients was measured by X-ray micro-computed tomography (X-ray μCT) (Ketcham and Carlson, 2001; Müller et al., 2009). Analyses were carried out on a drilled core, 1.4 cm in diameter and 3 cm in length, using a SkyScan 1173 high-resolution μCT scanner operated at 100 kV/80 μA, and a 1 mm Al-filter. Data collection consisted in the acquisition of 1600 X-ray shadow projections of the step-wise rotating sample (360° overall rotation in step of 0.225°). Shadow projections with a pixel size of 6.43 μm and an average of 25 frames (exposure time 800 ms) were taken for each rotational step.

Mineral chemistry was determined through wavelength dispersive analysis on a five spectrometer JEOL JXA-8200 SuperProbe electron microprobe analyzer (EMPA) operated at 15 kV/10 nA, with a 30 μm electron beam. Integrated counting times were 30/15 s (peak/background) for Ca and Fe and 60/30 s for Mg and Mn. Data were matrix-corrected using the CITZAF procedure formulated by Armstrong (1991). The detection limits for Mg, Mn and Fe were typically lower than 150 ppm. Natural carbonates and an MnTi-alloy were used as standards.

Trace element composition was measured by laser ablation-inductively coupled plasma-mass spectrometry (LA-ICP-MS). The instrument employed a pulsed ArF (193 nm) Lambda Physik NewWave UP-193-FX excimer laser with 6 J/cm^2 on-sample energy density at a repetition rate of 20 Hz coupled with an Element XR sector-field ICP-MS. The NIST-SRM612 glass was used as external standard, and CaO wt% (obtained by EMPA) was taken as internal standard. Analyses were performed with a round spot measuring 75 and 100 μm in diameter for calcite and dolomite, respectively. Data reduction was carried out with the LAMTRACE software (Longerich et al., 1996).

Stable isotope analyses (oxygen and carbon) were performed on hand-drilled powders of calcite and dolomite. The powders were extracted from a slightly stained slab, which was carefully cleaned prior to extraction. Between 150 and 450 μg were filled in sample vials and analyzed using a Gas-Bench coupled to a Finnigan Delta Plus XL mass spectrometer according to the method described in Spötl and Vennemann (2003).

The crystallographic orientations of calcite and dolomite were measured on a sample block ($1.5 \times 4 \times 1$ cm^3) by electron backscattered diffraction (EBSD; Venables and Harland, 1973; Prior et al., 1999). Simultaneous EDX-EBSD analyses were carried out using a Tescan Mira LMU FE-SEM operated at 15 kV, 23 mm working distance, 70° sample tilt, and equipped with a Nordlys S detector and the Oxford Instruments Channel 5.10 software package. To avoid possible misindexing of calcite grains by the dolomite match unit and vice versa, and because calcite and dolomite have similar lattices when considering the orientations of the *c*-axes (the structure of dolomite is similar to that of calcite except that Ca layers alternate with Mg layers along the *c*-axis), they were

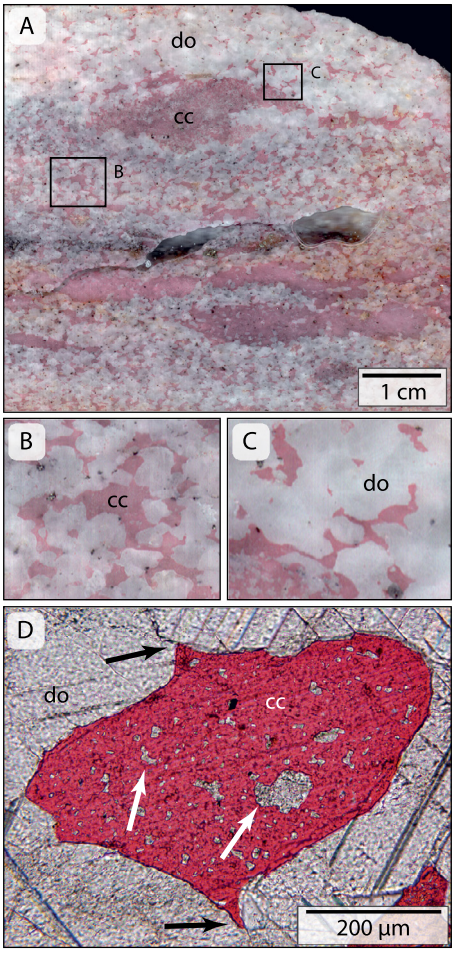

Fig. 3. (A) Stained slab of sample DF316 documenting the dolomite (white) and calcite (red) distribution. Calcite is either interstitial or crystallized in pockets. (B and C) Close-up views of (A) displaying the interconnected melt network of calcite and grain boundary triples junctions. (D) The stained thin section illustrates well the acute dihedral angles of the cc–do–do grain boundaries (black arrows) and dolomite exsolutions (white arrows).

both indexed using the same match unit (Althoff, 1977; American Mineralogist database). Both phases were discriminated from each other based on EDX data and placed in different subsets. Inverse pole figure (IPF) maps were noise-reduced using the wildspike correction method and a six-neighbor zero solution extrapolation.

4. Results

4.1. Microstructure

Calcite in sample DF316 occurs either as grains a few hundreds of µm in size within cm-scale pockets of calcite, or as a pervasive and interconnected network of interstitial grains within dolomite-rich regions (Fig. 3A; see also supplementary X-ray µCT images). Observations of stained slabs and reconstructions of X-ray µCT data show that interstitial calcite is connected by a network of narrow channels within a grain-supported dolomite framework (e.g. Figs. 3B and C). Calcite commonly displays concave grain-boundaries towards rounded dolomite grains. Calcite grains at calcite–dolomite–dolomite triple junctions have acute terminations suggesting low dihedral angles (Fig. 3D; black arrows). The actual cc–do–do dihedral angle of 28° (Fig. 4) was determined from 100 measurements of the apparent angle, from which the true angle was calculated following the method of Riegger and Van Vlack (1960).

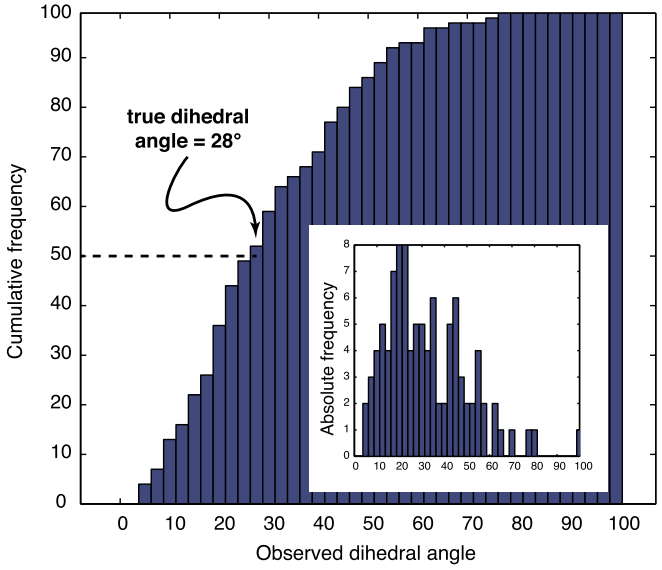

Fig. 4. Histogram displaying the cumulative frequencies of 100 cc–do–do dihedral angles measured in sample DF316. The true dihedral angle corresponds to the median value, according to Riegger and Van Vlack (1960). Absolute frequencies are shown in the small window for comparison.

Dolomite grains form a granoblastic fabric. Dolomite commonly shows twin lamellae, whereas most of calcite grains are non-twinned. In a few instances, dolomite crystal faces are well-developed. Secondary dolomite exsolutions are abundant in many calcite crystals. They form worm-like and sometimes oriented structures (Figs. 3D and Supplementary material Fig. S1).

4.2. Calcite–dolomite thermometry

The molar ratios of Mg (X_{Mg}) in calcite range between 0.018 and 0.108. This corresponds to temperatures of 325 and 692 °C (Supplementary material Fig. S2) using the calcite–dolomite thermometer of Anovitz and Essene (1987). The exsolution of dolomite from calcite leads to this large variation. Representative EMPA analyses of calcite and dolomite are given in the Supplementary material (Table 1).

To account for the dolomite exsolution we assumed that all dolomite present in a grain was exsolved from that calcite grain. Modal abundances of calcite and dolomite in a grain were determined from BSE images and multiplied by the average X_{Mg} composition of calcite (0.056, $n = 69$) and dolomite (0.485, $n = 38$), obtained from electron microprobe analysis. X_{Mg} values determined in this way range from 0.090 to 0.103, producing a tight temperature estimate of 651 to 681 °C (Supplementary material Table 2).

4.3. Trace element and stable isotope geochemistry of carbonates

Chondrite-normalized REE patterns of calcite and dolomite from sample DF316 show a negative slope from the LREE to the HREE (Supplementary material Fig. S3), with a strong Eu-anomaly and flat HREE patterns for calcite, and a weak Eu-anomaly and uneven HREE patterns for dolomite. Partition coefficients ($K_D^{cc/do}$) for five adjacent calcite–dolomite pairs are between 9–21 for the LREE and 12–35 for the HREE (Fig. 5, Supplementary material Table 3). Absolute REE concentrations range between 0.001 and 4.422 ppm. We could not find any correlation of trace element concentrations, with either crystallographic preferred orientations (CPO) or with the microstructure (interstitial calcite vs. calcite crystallized in pockets).

The results obtained from stable isotope analyses of carbonates are shown in Fig. 6. The $\delta^{18}O$ values for calcite vary between

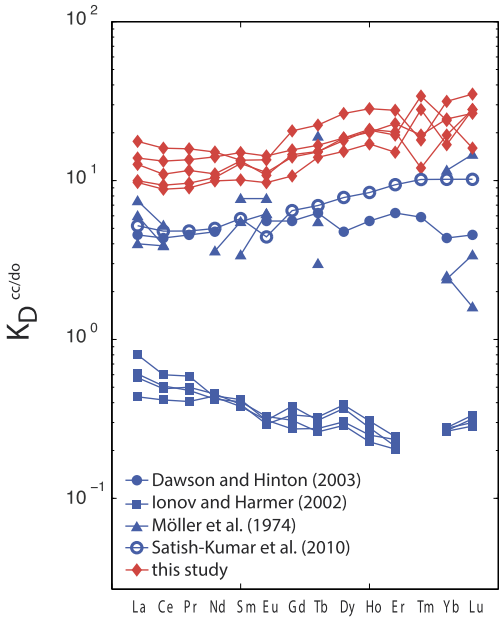

Fig. 5. Partition coefficients ($K_D^{cc/do}$) calculated for five adjacent calcite/dolomite pairs (red). The values are compared with data reported in the literature (blue). (For interpretation of the references to color in this figure legend, the reader is referred to the web version of this article.)

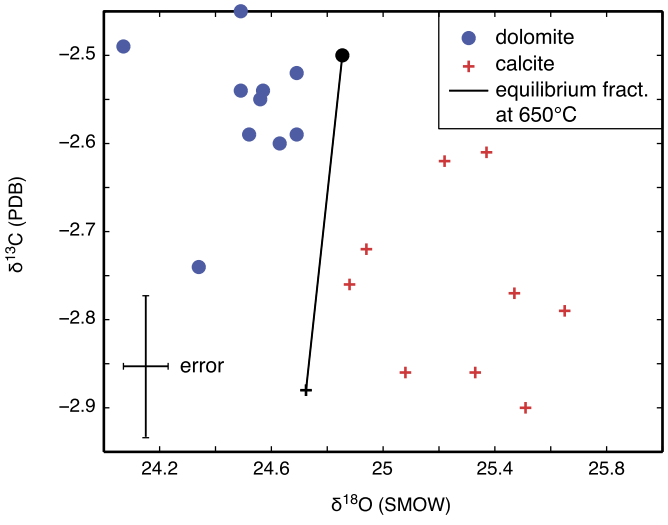

Fig. 6. Powders for oxygen and carbon isotopic analysis were sampled from a single sample, which was slightly stained to identify the calcite grains. The observed fractionation between calcite and dolomite grains for $\delta^{18}O$ and $\delta^{13}C$ values indicates isotopic disequilibrium. A fictive equilibrium pair is indicated by the solid line given on the diagram, calculated for 650 °C.

24.9 and 25.7‰, whereas the $\delta^{13}C$ values range between −2.6 and −2.9‰. Dolomite grains have slightly lower $\delta^{18}O$ values (24.1 and 24.7‰), and almost identical $\delta^{13}C$ values (−2.4 and −2.7‰). The black line shows the equilibrium fractionation between calcite and dolomite at 650 °C for the carbon and oxygen isotopic exchanges (Sheppard and Schwarcz, 1970). The $\delta^{18}O$ of calcite and dolomite are non-overlapping populations with $\delta^{18}O(cc) > \delta^{18}O(do)$. By anyone's estimation, this is a reverse fractionation that proves disequilibrium between calcite and dolomite in terms of oxygen isotope exchange (e.g. Zheng, 1999). Indeed, measured compositions are typical for Triassic dolomites (Hoefs, 2009). This precludes infiltration of large amounts of fluids emanating from the intrusion or large hydrothermal convections (e.g. Baumgartner and Valley, 2001), which both would change the isotopic composition towards much lower values.

4.4. Crystallographic preferred orientation of carbonates

The crystallographic preferred orientations (CPO) measured by EBSD show an obvious clustering of dolomite *c*-axes normal to the foliation plane (Fig. 7A). This CPO arises from dislocation glide on the basal c(0001) plane of the crystal lattice (Barber et al., 1981), a feature commonly observed in polycrystalline dolomite deformed at high-T under uni-axial compression (e.g. Wenk and Shore, 1975; Barber et al., 1994).

Calcite shows a bimodal distribution of *c*-axes. Interstitial calcite has a similar CPO as dolomite, i.e. with *c*-axes oriented normal to the foliation (Fig. 7B). The CPO is less well defined, as indicated by the broader dispersion of *c*-axes and the lower maximum contour value (m.u.d. value) for calcite, when compared with dolomite. According to Wenk et al. (1983 and 1987), CPO with *c*-axes oriented normal to the foliation plane, i.e. parallel to the compression direction, is characteristic for low-T deformation. Unlike interstitial grains, calcite unambiguously attributed to melt pockets shows a strong clustering of *c*-axes parallel to the foliation plane, at right angle to the CPO of dolomite and interstitial calcite (Fig. 7C).

5. Discussion

5.1. Microstructures produced by melting

The acute dihedral angles observed in the carbonates (Fig. 3) are typical for the presence of a melt phase (e.g. Cooper and Kohlstedt, 1982; Jurewicz and Watson, 1984; Sawyer, 1999). The low true dihedral angle (28°) measured for cc–do–do triple junctions corresponds to a value expected if calcite formed by crystallization from a carbonate melt, although no experimental measurements of cc-melt with dolomite are available. However, dihedral angles of 28° and 25–30° are reported for olivine with melts of dolomitic (Hunter and McKenzie, 1989) and Na-carbonitic (Minarik and Watson, 1995) compositions, respectively. In contrast, dihedral angles for salt-rich fluids with carbonates were determined, and yield values between 45 and 80° (see review in Brenan, 1991). Hence, the low values seen here are in agreement with melt, rather than fluid. Further, the high temperatures obtained from cc–do thermometry and the exsolution of dolomite from calcite preclude that the interstitial calcite was precipitated by infiltration of a low-temperature, post-intrusive Ca-rich fluid.

Low dihedral angles in a porous media may lead to the formation of an interconnected melt network (e.g. Brenan, 1991). This is well seen in the X-ray tomography images, which collaborate the thin section observations (Supplementary material movie). Similar textures were seen by Wohlers and Baumgartner (2013) in the Little Cottonwood aureole, where pegmatite-forming melts infiltrated quartzites, leading to an interconnected network.

5.2. Calcite–dolomite disequilibrium as indicator for partial melting

The textures discussed above are disequilibrium grain boundary features between calcite and dolomite since they preserve textural equilibration between a carbonate melt and dolomite. Indeed, the data presented above suggests that a (geochemical) disequilibrium between calcite and dolomite was preserved, since the calcite crystallizing from melt did not equilibrate with the dolomite crystals.

The partition coefficients between calcite and dolomite ($K_D^{cc/do}$) measured in this study (LREE: 9–21; HREE: 12–35) for adjacent calcite–dolomite pairs are significantly higher than those reported in the literature for equilibrated mineral pairs (Fig. 5). $K_D^{cc/do}$ smaller than 10 are commonly observed in regional metamorphic marbles (Möller et al., 1974; Satish-Kumar et al., 2010), and carbonatites (Dawson and Hinton, 2003; Ionov and Harmer, 2002). Model calculations using the ionic radii of some trace elements

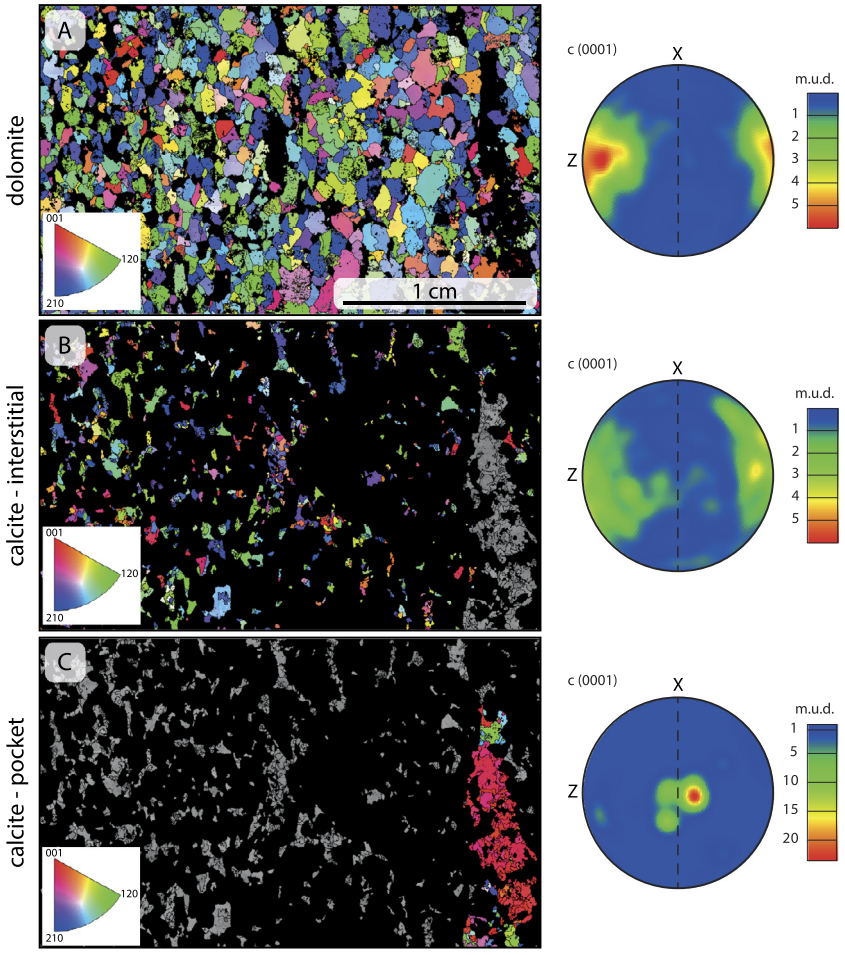

Fig. 7. EBSD Inverse pole figure (IPF) maps (left) illustrating the crystallographic axes for (A) dolomite, (B) interstitial calcite and (C) calcite localized in melt pockets. The corresponding pole figures are shown on the right. Dolomite and interstitial calcite *c*-axes are oriented parallel to Z (normal to foliation plane; bluish to greenish colors in IPF maps), whereas *c*-axes for calcite from the melt pockets are clustered parallel to Y (within the foliation plane; reddish color in IPF map). Pole figures are represented on lower hemisphere equal area projections and the texture strength is expressed by multiples of the uniform distribution (m.u.d.) calculated using a Gaussian half-width of 15. The rock foliation (XY plane) is shown by a dashed line. (For interpretation of the references to color in this figure legend, the reader is referred to the web version of this article.)

and the carbonate structures suggest even smaller $K_D^{cc/do}$ values of less than 2 (Kretz, 1982).

In contrast, trace elements seem to favor the carbonate melt strongly. Preferential partitioning of trace elements into the melt phase was observed in melting experiments of calcite (Durand and Baumgartner, 2008). Ionov and Harmer (2002) suggested the same trace element behavior for interstitial carbonates with respect to phenocrysts in carbonatites. Similarly, Korsakov and Hermann (2006) interpreted polyphase inclusions in garnet and clinopyroxene as trapped carbonate melts based on their trace element concentrations. The carbonate inclusions are enriched in LREE and depleted in HREE with respect to matrix carbonates. We argue that the trace element concentrations in calcite of the studied sample are high, because the melt had concentrated them. The melt does not exchange with the remaining dolomite crystals on crystallization, leaving the calcite enriched in trace elements.

Indeed, stable isotope analyses further support a disequilibrium precipitation of calcite. The black line in Fig. 6 shows the expected equilibrium fractionation of $\delta^{18}O$ and $\delta^{13}C$ for a sub-solidus assemblage of calcite and dolomite at 650 °C. At equilibrium, calcite should have lower $\delta^{18}O$ values than dolomite. To our knowledge there are no published cc-melt – dolomite fractionation factors for oxygen. The measured values could represent the equilibrium fractionation between dolomite and a calcite rich melt. Indeed, one would expect a very small fractionation factor between melt and carbonate, similar to the one between silicates and melt (<1–2‰; see review in Eiler, 2001). Again, we would argue, that during cooling the melt did not equilibrate upon crystallizing with the dolomite. In addition, such disequilibrium could be the result of melt-infiltration derived from a slightly different protolith. In any case, no complete re-equilibration was achieved during cooling.

Ferry et al. (2011) reported similar results in contact metamorphosed siliceous dolomites. Calcite from samples estimated at 680 °C and 690 °C (thus above the solidus) have higher $\delta^{18}O$ values than adjacent dolomite (samples B4L and B1W of Ferry et al., 2011). The disequilibrium in this case could result from partial melting of the carbonate. In contrast, $\delta^{18}O$ for calcite and dolomite from a sample estimated at ~595 °C (below melting conditions) are uniform. No partial melting is expected in this case and the isotopes are consistent with the predicted equilibrium fractionation.

5.3. Partial melting supported by crystallographic preferred orientations

The difference in *c*-axes orientation between calcite in different locations is striking. The orientation of *c*-axes observed for interstitial calcite is similar to that of dolomite, i.e. normal to the foliation plane, while calcite in melt pockets has *c*-axes oriented normal to those of dolomite. These differences likely arise because calcite was largely molten during deformation in the pockets, and hence

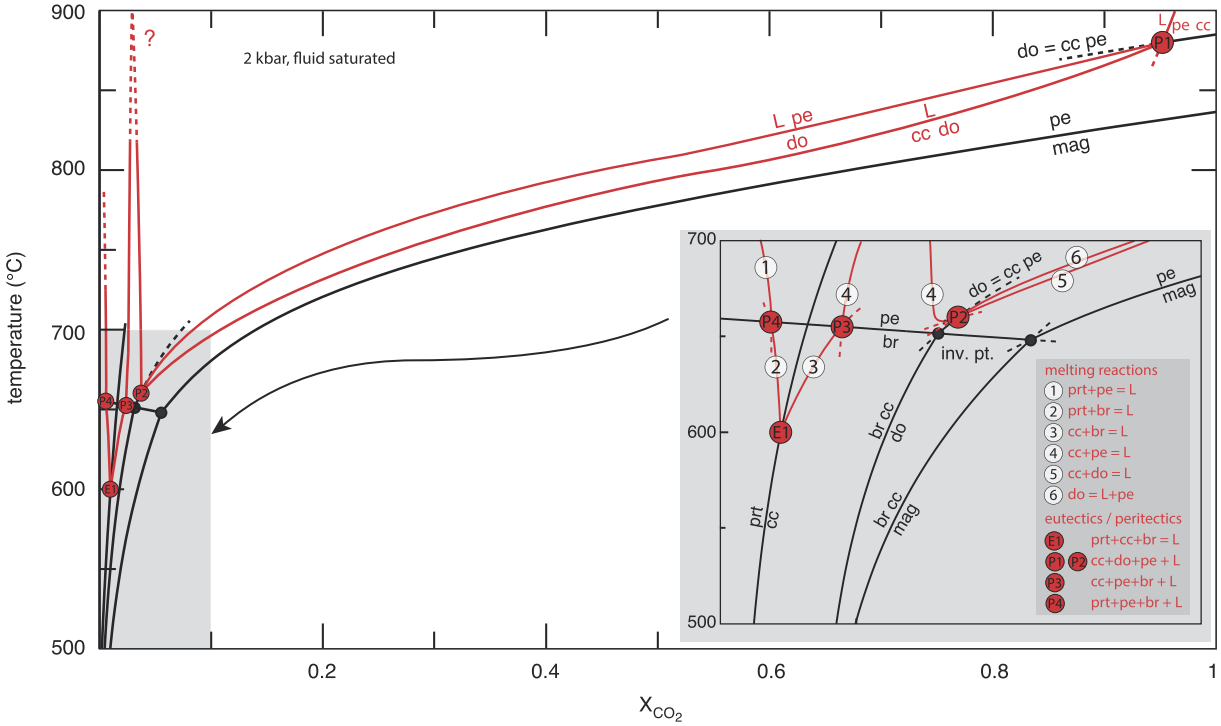

Fig. 8. T–X(CO_2) Schreinemaker projection showing carbonate melting reactions (red lines) and solid reactions (black lines). The region around the lowest temperature eutectic (E1) has been modified after Wyllie (1965) and the region around the peritectics (P1 and P2) has been interpreted based on the data of Fanelli et al. (1986). A vapor phase (+V) is present everywhere in the diagram (e.g. the phase diagram was calculate for vapor saturation). The solid reactions were calculated using PerpleX (Connolly, 2009) with the HP04 thermodynamic database (Holland and Powell, 1998), with the exception of the estimated position of the reaction prt = cc, for which no thermodynamic data are available. Abbreviations are: calcite (cc), dolomite (do), magnesite (mag), portlandite (prt), brucite (br), periclase (pe). (For interpretation of the references to color in this figure legend, the reader is referred to the web version of this article.)

incapable to adapt the CPO. Assuming a solid assemblage of calcite and dolomite, a similar CPO (even though not automatically of equal strength) would have been expected after deformation (Delle Piane et al., 2009).

The stronger CPO of dolomite may be explained by the fact that dolomite was never molten, thus enabling a more complete record of the rock deformation history. In contrast, interstitial calcite was molten during the emplacement of the intrusive body and only recorded parts of the deformation process. Twinning is much more widespread in dolomite and supports the idea of late crystallization of calcite at the end of the deformation phase.

The peculiar CPO of calcite from the melt pockets, with *c*-axes oriented within the foliation plane (i.e. normal to that of dolomite and interstitial calcite) suggests that it did not crystallize associated with compressional stress during the intrusion, but rather formed after deformation had stopped or in another deformation regime. Katz and Keller (1981) showed that statically grown calcite grew with *c*-axes oriented parallel to the dike walls in carbonatite dikes from the Kaiserstuhl (Germany). Calcite from the melt pockets could have behaved the same way and crystallized with *c*-axes parallel to the pocket walls after the main deformation stage. Since the melt pocket walls are parallel to the foliation, this would explain the non-random texture of calcite located in melt pockets.

6. Thermodynamic analysis and P–T–X conditions for partial melting

Various attempts have been made in the literature to provide phase diagrams for partial melting of carbonates in the crust in the presence of fluids (e.g. Lentz, 1999; Wenzel et al., 2001; Lee and Wyllie, 1998). The attempts are based on the experimental work of Wyllie and co-workers (e.g. Fanelli et al., 1986; Wyllie, 1965). Here we build on the work of Fanelli et al. (1986), which is by far the most comprehensive discussion of experiments in the CaO–MgO–CO_2–H_2O system, with most data given at 2 kbar.

We have constructed a quantitative temperature-X(CO_2)$_{fluid}$ diagram (Fig. 8) to which we added in a qualitative manner the reactions involving melt based on Fanelli et al. (1986). A T–X(CO_2) Schreinemaker diagram was calculated for the system CaO–MgO–CO_2–H_2O, assuming fluid saturation, using the PerpleX software (Connolly, 2009) with the HP04 database of Holland and Powell (1998). No thermodynamic data are available for carbonate melt. We used the reported temperatures of E1, P1 and P2 (Fig. 1). E1 is located on the portlandite–calcite reaction at 600 °C, while P1 (880 °C) and P2 (650 °C) were placed on the reaction do → pe + cc + CO_2 (Fanelli et al., 1986). A Schreinemaker analysis reveals that there are several possible configurations of the reactions around P1 and P2, depending on the composition of the melt. Adopting as closely as possible the temperatures of Fanelli et al. (1986) for P1 and P2, and combining them with the calculated T–X(CO_2) for melt absent reactions leaves very little freedom in drawing the melting curves. Finally, Fanelli et al. (1986) estimate the temperature of the maximum of the melting reaction between P2 and P3 to be ~900 °C, involving calcite, periclase, liquid and vapor.

The diagram in Fig. 8 shows that partial melting is expected over a vast range of fluid compositions, essential through reaction 5 (cc + do → L) and reaction 6 (do → pe + L). The scarcity of periclase (or corresponding alteration products) in the samples of the present study suggests that reaction 5 was the melt-producing reaction in the Adamello contact aureole. Melting at the extremely high water-rich compositions necessary for E1 is possible, though the absence of portlandite in nearly all contact aureoles argues against this occurring naturally. It would require huge amounts of nearly pure-water infiltration. Fluid compositions larger than that of P2 (~0.05 X$_{CO_2}$) will result in partial melting of carbonates at

temperatures above 650 °C. For example, the prograde path of a closed system with small porosity (≪1%) is given by cc + do → cc + do + br → cc + do + br + pe (invariant point) → cc + do + pe. Up to this point, only vanishingly small amounts of the phases pe or br are formed (Baumgartner and Ferry, 1991). Infiltration of an H_2O-rich fluid can, at this temperature produce the assemblage cc + pe ± do, ubiquitously found in contact aureoles (e.g. Moore and Kerrick, 1976; Cook and Bowman, 2000; Ferry et al., 2002; Nabelek, 2002; Müller et al., 2009). If sufficient amounts of fluid infiltrate, all dolomite reacts to form cc + pe, and partial melting will only occur at very high temperatures. In contrast, a further increase of temperature without infiltration will buffer the fluid to P2, where very small amounts of melt are produced. Here, a fluid infiltration will increase the amount of melt. Only very large amounts of fluid are expected to yield a significant isotopic shift (Baumgartner and Rumble, 1988; Ferry and Gerdes, 1998), a feature we did not observe in the Adamello rocks. The large range of fluid compositions and temperatures for which partial melting of carbonates is expected, suggests that it could be observed not only in contact aureoles but also in regional metamorphic settings.

7. Implications

Partial melting of carbonates, up to now considered marginal or non-existent, might be more common than previously thought. The presence of a carbonate melt in crustal levels has several implications for various geologic disciplines. The main implications involve modifications of (1) fluid flow dynamics and (2) deformation behavior.

Aqueous fluids are generated and expulsed from a crystallizing intrusion (e.g. Hanson, 1995). If porosities are high enough, a convection regime may be established (e.g. Gerdes et al., 1998; Cui et al., 2001; Fu et al., 2010) and infiltrated carbonates are likely to melt. This results potentially in a complex two-phase flow environment, clogging the system (e.g. Driesner and Geiger, 2007) and hindering extensive fluid flow close to the intrusion. The convective system may regenerate after crystallization of the partially molten carbonates. Fluids ejected upon solidification of the carbonates will likely obliterate much of the textural evidence. In addition, melting of large amounts of carbonates might accelerate the solidification of intrusions. Carbonates melt at temperatures below the fluid-saturated minimum of silicic systems (e.g. Johannes and Holtz, 1996), and thus represent a significant energy sink.

Another reason for the fact that silicic intrusions are frequently hosted in carbonates is the important rheological contrast, which is even more accentuated if they are partially molten. The viscosity of carbonate rocks can be calculated using flow laws determined in deformation experiments, and input parameters such as temperature, grain size, stress and strain rate. Assuming a temperature of 700 °C, stress $\sigma = 100$ MPa, grain size $d = 500$ µm and strain rate $\gamma = 10^{-10}$, a viscosity of log $\eta_{\text{eff}} = 16$ Pa s is obtained using the flow law of Delle Piane et al. (2008) (Fig. 9). The presence of melt causes a drastic drop in rock viscosity of several orders of magnitude, which is maximal for a rheologically critical melt fraction (RCMF) of ~0.25–0.30 (Scott and Kohlstedt, 2006). For melt fractions above the RCMF, the viscosity can be approximated by the Einstein–Roscoe equation (Roscoe, 1952) or the parameterization by Costa et al. (2009). No data are available for melt fractions below the RCMF. Viscosities of 10^0 to 10^{-3} Pa s are reached for fully molten carbonates (Wolff, 1994; Jones et al., 1995).

Thus, partially molten carbonates have the same viscosity range as silicic intrusions (10^4–10^{12} Pa s), whereas carbonate melt viscosities are several orders of magnitude smaller. Squeezing out the highly mobile carbonate melt thus provides a tangible explanation for the space-making issue related to the emplacement of intrusions. Indeed, the emplacement of the Western Adamello Tonalite may have been partially accommodated by squeezing out of the carbonate melt, resulting in an extreme thinned sequence. A layer of pure dolomite in contact with the silicic intrusion could represent the restite, left behind after calcitic melting and extraction occurred. Provided all melt was extracted and heating and fluid infiltration would have continued, a restite composed of periclase is obtained. This was observed by Wenzel et al. (2001). Further, we find host rocks that have been infiltrated by a carbonate melt in the somewhat more distal sedimentary sequence. These calcite-bearing samples show a much weaker CPO than the sample presented in this study (Floess, 2013).

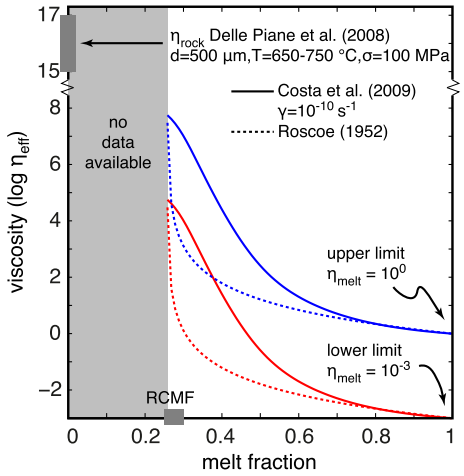

Fig. 9. Diagram illustrating the extreme range of viscosities encountered in partially molten carbonates as a function of melt fraction. The blue and red curves are calculated for a melt viscosity of 10^0 and 10^{-3} Pa s, respectively. (For interpretation of the references to color in this figure legend, the reader is referred to the web version of this article.)

8. Summary

We have presented and discussed arguments documenting the partial melting of carbonates in the Western Adamello contact aureole. The T–X(CO_2) diagram using published experimental data and a Schreinemaker analysis for the system CaO–MgO–CO_2–H_2O predict the onset of melting at temperatures around 600–650 °C, and thus suggest that this might be a more common process than previously thought. Key implications are (1) a drastic drop in viscosity, causing deformation localization and facilitated emplacement of intrusions and (2) modification/inhibition of fluid flow around igneous intrusions. The combination of microstructural, textural and geochemical methods provides direct criteria for evaluation of partial melting in carbonate rocks in other localities.

Acknowledgements

We thank Othmar Müntener, Tom Foster and John Bowman for fruitful discussions and comments. Further we thank Alexey Ulianov and Thorsten Vennemann for lab access and discussions. The constructive reviews and suggestions by Dave Pattison and John Ferry, and the editorial handling and comments by Tim Elliott significantly improved the manuscript. This research was funded by the Swiss National Science Foundation grant “Pro-Doc Adamello” PDFMP2-123081. We thank the “Parco dell’Adamello” for giving permission to collect samples.

Appendix A. Supplementary material

Supplementary material related to this article can be found online at http://dx.doi.org/10.1016/j.epsl.2014.10.031.

References

Althoff, P.L., 1977. Structural refinements of dolomite and a magnesian calcite and implications for dolomite formation in the marine environment. Am. Mineral. 62, 772–783.

Anovitz, L.M., Essene, E.J., 1987. Phase equilibria in the system $CaCO_3$–$MgCO_3$–$FeCO_3$. J. Petrol. 28, 389–415.

Armstrong, J., 1991. Quantitative elemental analysis of individual microparticles with electron beam instruments. In: Heinrich, K.F.J., Newbury, D.E. (Eds.), Electron Probe Quantitation. Plenum Press, pp. 261–315.

Barber, D.J., Heard, H.C., Wenk, H.R., 1981. Deformation of dolomite single-crystals from 20–800 °C. Phys. Chem. Miner. 7, 271–286.

Barber, D.J., Wenk, H.-R., Heard, H.C., 1994. The plastic deformation of polycrystalline dolomite: comparison of experimental results with theoretical predictions. Mater. Sci. Eng. A 175, 83–104.

Baumgartner, L.P., Ferry, J.M., 1991. A model for coupled fluid-flow and mixed-volatile mineral reactions with applications to regional metamorphism. Contrib. Mineral. Petrol. 106, 273–285.

Baumgartner, L.P., Rumble III, D., 1988. Transport of stable isotopes: I: development of a kinetic continuum theory for stable isotope transport. Contrib. Mineral. Petrol. 98, 417–430.

Baumgartner, L.P., Valley, J.W., 2001. Stable isotope transport and contact metamorphic fluid flow. Rev. Mineral. Geochem. 43, 415–467.

Brack, P., 1984. Geologie der Intrusiva und Rahmengesteine des Südwest-Adamello (Nord-Italien). PhD thesis. ETH, Zürich. 253 pp.

Brack, P., Dal Piaz, G.V., Baroni, C., Carton, A., Nardin, M., Pellegrini, G.B., Pennacchioni, G., 2008. Note illustrative della Carta Geologica d'Italia alla scala 1:50.000: foglio 058 – Monte Adamello. APAT, Servizio Geologico d'Italia. 140 pp.

Brenan, J., 1991. Development and maintenance of metamorphic permeability, implications for fluid transport. Rev. Mineral. Geochem. 26, 291–319.

Connolly, J.A.D., 2009. The geodynamic equation of state: what and how. Geochem. Geophys. Geosyst. 10.

Cook, S.J., Bowman, J.R., 2000. Mineralogical evidence for fluid–rock interaction accompanying prograde contact metamorphism of siliceous dolomites: Alta Stock Aureole, Utah, USA. J. Petrol. 41, 739–757.

Cooper, R.F., Kohlstedt, D.L., 1982. Interfacial energies in the olivine–basalt system. Adv. Earth Planet. Sci. 12, 217–228.

Costa, A., Caricchi, L., Bagdassarov, N., 2009. A model for the rheology of particle-bearing suspensions and partially molten rocks. Geochem. Geophys. Geosyst. 10, 1–13.

Cui, X., Nabelek, P.I., Liu, M., 2001. Heat and fluid flow in contact metamorphic aureoles with layered and transient permeability, with application to the Notch Peak aureole, Utah. J. Geophys. Res. 106, 6477.

Dawson, J.B., Hinton, R.W., 2003. Trace-element content and partitioning in calcite, dolomite and apatite in carbonatite, Phalaborwa, South Africa. Mineral. Mag. 67, 921–930.

Delle Piane, C., Burlini, L., Kunze, K., Brack, P., Burg, J.P., 2008. Rheology of dolomite: large strain torsion experiments and natural examples. J. Struct. Geol. 30, 767–776.

Delle Piane, C., Burlini, L., Kunze, K., 2009. The influence of dolomite on the plastic flow of calcite: rheological, microstructural and chemical evolution during large strain torsion experiments. Tectonophysics 467, 145–166.

Driesner, T., Geiger, S., 2007. Numerical simulation of multiphase fluid flow in hydrothermal systems. Rev. Mineral. Geochem. 65, 187–212.

Durand, C., Baumgartner, L.P., 2008. Experimentally major and trace partitioning between calcitic melt and calcite at 1000 bars. Geochim. Cosmochim. Acta 72, A234.

Eiler, J.M., 2001. Oxygen isotope variations of basaltic lavas and upper mantle rocks. Rev. Mineral. Geochem. 43, 319–364.

Fanelli, M., Cava, N., Wyllie, P.J., 1986. Calcite and dolomite without portlandite at a new eutectic in CaO–MgO–CO_2–H_2O, with applications to carbonatites. In: Presented at the Morphology and Phase Equilibria of Minerals: Proceedings of the 13th General Meeting of the International Mineralogical Association. Sofia, Bulgarian Academy of Science, pp. 313–322.

Ferry, J., Gerdes, M., 1998. Chemically reactive fluid flow during metamorphism. Annu. Rev. Earth Planet. Sci. 26, 255–287.

Ferry, J.M., Wing, B.A., Penniston-Dorland, S.C., Rumble, D., 2002. The direction of fluid flow during contact metamorphism of siliceous carbonate rocks: new data for the Monzoni and Predazzo aureoles, northern Italy, and a global review. Contrib. Mineral. Petrol. 142, 679–699.

Ferry, J.M., Ushikubo, T., Valley, J.W., 2011. Formation of forsterite by silicification of dolomite during contact metamorphism. J. Petrol. 52, 1619–1640.

Floess, D., 2013. Contact metamorphism and emplacement of the Western Adamello Tonalite. PhD thesis. University of Lausanne. 208 pp.

Fu, F.Q., McInnes, B., Evans, N.J., Davies, P.J., 2010. Numerical modeling of magmatic-hydrothermal systems constrained by U–Th–Pb–He time-temperature histories. J. Geochem. Explor. 106, 90–109.

Gerdes, M.L., Baumgartner, L.P., Person, M., 1998. Convective fluid flow through heterogeneous country rocks during contact metamorphism. J. Geophys. Res. 103, 23983–24003.

Hanson, R.B., 1995. The hydrodynamics of contact metamorphism. Geol. Soc. Am. Bull. 107, 595–611.

Hoefs, J., 2009. Stable Isotope Geochemistry, 6th ed. Springer. 285 pp.

Holland, T., Powell, R., 1998. An internally consistent thermodynamic data set for phases of petrological interest. J. Metamorph. Geol. 16, 309–343.

Hunter, R.H., McKenzie, D., 1989. The equilibrium geometry of carbonate melts in rocks of mantle composition. Earth Planet. Sci. Lett. 92, 347–356.

Hutchison, C., 1974. Laboratory Handbook of Petrographic Techniques. J. Wiley & Sons, New York. 527 pp.

Ionov, D.A., Harmer, R.E., 2002. Trace element distribution in calcite–dolomite carbonatites from Spitskop: inferences for differentiation of carbonatite magmas and the origin of carbonates in mantle xenoliths. Earth Planet. Sci. Lett. 198, 495–510.

Johannes, W., Holtz, F., 1996. Petrogenesis and Experimental Petrology of Granitic Rocks. Springer, Berlin and New York.

Johnson, T.E., Gibson, R.L., Brown, M., Buick, I.S., Cartwright, I., 2003. Partial melting of metapelitic rocks beneath the Bushveld Complex, South Africa. J. Petrol. 44, 789–813.

Jones, A.P., Dobson, D.P., Genge, M., 1995. Comment on physical properties of carbonatite magmas inferred from molten salt data, and application to extraction patterns from carbonatite–silicate magma chambers. Geol. Mag. 132, 121.

Jurewicz, S.R., Watson, E.B., 1984. Distribution of partial melt in a felsic system: the importance of surface energy. Contrib. Mineral. Petrol. 85, 25–29.

Jutras, P., Macrae, A., Owen, J., Dostal, J., 2006. Carbonate melting and peperite formation at the intrusive contact between large mafic dykes and clastic sediments of the upper Palaeozoic Saint-Jules Formation, New-Carlisle, Quebec. Geol. J. 41, 23–48.

Katz, K., Keller, J., 1981. Comb-layering in carbonatite dykes. Nature 294, 350–352.

Ketcham, R.A., Carlson, W.D., 2001. Acquisition, optimization and interpretation of X-ray computed tomographic imagery: applications to the geosciences. Comput. Geosci. 27, 381–400.

Korsakov, A.V., Hermann, J., 2006. Silicate and carbonate melt inclusions associated with diamonds in deeply subducted carbonate rocks. Earth Planet. Sci. Lett. 241, 104–118.

Kretz, R., 1982. A model for the distribution of trace-elements between calcite and dolomite. Geochim. Cosmochim. Acta 46, 1979–1981.

Lee, W.J., Wyllie, P.J., 1998. Processes of crustal carbonatite formation by liquid immiscibility and differentiation, elucidated by model systems. J. Petrol. 39, 2005–2013.

Lentz, D.R., 1999. Carbonatite genesis: a reexamination of the role of intrusion-related pneumatolytic skarn processes in limestone melting. Geology 27, 335–338.

Longerich, H.P., Jackson, S.E., Günther, D., 1996. Inter-laboratory note. Laser ablation inductively coupled plasma mass spectrometric transient signal data acquisition and analyte concentration calculation. J. Anal. At. Spectrom. 11, 899.

Minarik, W.G., Watson, E.B., 1995. Interconnectivity of carbonate melt at low melt fraction. Earth Planet. Sci. Lett. 133, 423–437.

Möller, P., Parekh, P., Morteani, G., 1974. Petrographic and trace-element distribution studies on the dolomite–calcite in the regional metamorphic marble of the Griesscharte, Tyrol, Austria/Italy. Chem. Geol. 13, 81–96.

Moore, J.N., Kerrick, D.M., 1976. Equilibria in siliceous dolomites of the Alta aureole, Utah. Am. J. Sci. 276, 502–524.

Müller, T., Baumgartner, L.P., Foster, C.T., Bowman, J.R., 2009. Crystal size distribution of periclase in contact metamorphic dolomite marbles from the Southern Adamello Massif, Italy. J. Petrol. 50, 451–465.

Nabelek, P.I., 2002. Calc-silicate reactions and bedding-controlled isotopic exchange in the Notch Peak aureole, Utah: implications for differential fluid fluxes with metamorphic grade. J. Metamorph. Geol. 20, 429–440.

Pattison, D.R.M., Harte, B., 1988. Evolution of structurally contrasting anatectic migmatites in the 3-kbar Ballachulish aureole, Scotland. J. Metamorph. Geol. 6, 475–494.

Pattison, D.R.M., Harte, B., 1997. The geology and evolution of the Ballachulish Igneous Complex and aureole. Scott. J. Geol. 33, 1–29.

Pennacchioni, G., Di Toro, G., Brack, P., Menegon, L., Villa, I.M., 2006. Brittle–ductile–brittle deformation during cooling of tonalite (Adamello, Southern Italian Alps). Tectonophysics 427, 171–197.

Prior, D.J., Boyle, A.P., Brenker, F., Cheadle, M.C., Day, A., Lopez, G., Peruzzi, L., Potts, G., Reddy, S., Spiess, R., 1999. The application of electron backscatter diffraction and orientation contrast imaging in the SEM to textural problems in rocks. Am. Mineral. 84, 1741–1759.

Riegger, O.K., Van Vlack, L.H., 1960. Dihedral angle measurement. Trans. Metall. Soc. AIME 218, 933–935.

Roscoe, R., 1952. The viscosity of suspensions of rigid spheres. Br. J. Appl. Phys. 3, 267–269.
Satish-Kumar, M., Hermann, J., Miyamoto, T., Osanai, Y., 2010. Fingerprinting a multistage metamorphic fluid–rock history: evidence from grain scale Sr, O and C isotopic and trace element variations in high-grade marbles from East Antarctica. Lithos 114, 217–228.
Sawyer, E.W., 1999. Criteria for the recognition of partial melting. Phys. Chem. Earth 24, 269–279.
Schneider, C., Rasband, W., Eliceiri, K., 2012. NIH Image to ImageJ: 25 years of image analysis. Nat. Methods 9, 671–675.
Scott, T., Kohlstedt, D.L., 2006. The effect of large melt fraction on the deformation behavior of peridotite. Earth Planet. Sci. Lett. 246, 177–187.
Sheppard, S.M.F., Schwarcz, H.P., 1970. Fractionation of carbon and oxygen isotopes and magnesium between coexisting metamorphic calcite and dolomite. Contrib. Mineral. Petrol. 26, 161–198.
Spötl, C., Vennemann, T.W., 2003. Continuous-flow isotope ratio mass spectrometric analysis of carbonate minerals. Rapid Commun. Mass Spectrom. 17, 1004–1006.
Venables, J.A., Harland, C.J., 1973. Electron back-scattering patterns—a new technique for obtaining crystallographic information in the scanning electron microscope. Philos. Mag. 27, 1193–1200.
Wenk, H.R., Shore, J., 1975. Preferred orientation in experimentally deformed dolomite. Contrib. Mineral. Petrol. 50, 115–126.
Wenk, H.-R., Barber, D.J., Reeder, R.J., 1983. Microstructures in carbonates. In: Reeder, R.J. (Ed.), Carbonates: Mineralogy and Chemistry. In: Reviews in Mineralogy, vol. 11. Mineralogical Society of America, pp. 301–367.
Wenk, H.R., Takeshita, T., Bechler, E., Erskine, B.G., Matthies, S., 1987. Pure shear and simple shear calcite textures – comparison of experimental, theoretical and natural data. J. Struct. Geol. 9, 731–745.
Wenzel, T., Baumgartner, L.P., Brügmann, G., Konnikov, E.G., Kislov, E.V., Orsoev, D.A., 2001. Contamination of mafic magma by partial melting of dolomitic xenoliths. Terra Nova 13, 197–202.
Wohlers, A., Baumgartner, L.P., 2013. Melt infiltration into quartzite during partial melting in the Little Cottonwood Contact Aureole (UT, USA): implication for xenocryst formation. J. Metamorph. Geol. 31, 301–312.
Wolff, J.A., 1994. Physical properties of carbonatite magmas inferred from molten salt data, and application to extraction patterns from carbonatite–silicate magma chambers. Geol. Mag. 131, 145–153.
Wyllie, P.J., 1965. Melting relationships in system CaO–MgO–CO_2–H_2O with petrological applications. J. Petrol. 6, 101–123.
Wyllie, P.J., Tuttle, O.F., 1959. Melting of calcite in the presence of water. Am. Mineral. 44, 453–459.
Wyllie, P.J., Tuttle, O.F., 1960. The system CaO–CO_2–H_2O and the origin of carbonatites. J. Petrol. 1, 1–46.
Zheng, Y.F., 1999. Oxygen isotope fractionation in carbonate and sulfate minerals. Geochem. J. 33, 109–126.